

2nd Symposium on New Trends in Nuclear and Medical Physics, Poland, September 24–26, 2025

Feasibility of $\bar{\text{H}}$ Annihilation-Vertex Reconstruction with Modular J-PET: A Simulation-Based Study

P. PANDEY^{a,b,*}, S. SHARMA^{a,b}, P. MOSKAL^{a,b}, R.C. FERGUSON^{c,d},
R. CARAVITA^{c,d} (ON BEHALF OF THE AE \bar{g} IS COLLABORATION),
A.K. VENADAN^{a,b}, G. KORCYL^{a,b} AND K. KACPRZAK^{a,b}

^aMarian Smoluchowski Institute of Physics, Jagiellonian University, prof. S. Łojasiewicza 11, 30-348 Kraków, Poland

^bCentre for Theranostics, Jagiellonian University, Kopernika 40, 31-501 Kraków, Poland

^cDepartment of Physics, University of Trento, Via Sommarive 14, 38123 Povo, Trento, Italy

^dINFN/TIFPA — Trento Institute for Fundamental Physics and Applications, Via Sommarive 14, 38123 Povo, Trento, Italy

Doi: [10.12693/APhysPolA.148.S169](https://doi.org/10.12693/APhysPolA.148.S169)

*e-mail: piyush.pandey@doctoral.uj.edu.pl

The Antihydrogen Experiment: gravity, Interferometry, Spectroscopy at CERN aims to measure the gravitational acceleration of antihydrogen ($\bar{\text{H}}$) atoms to test the weak equivalence principle for anti-matter systems. In the proposed approach, a pulsed $\bar{\text{H}}$ beam, produced via charge exchange between Rydberg positronium and antiprotons, traverses a moiré deflectometer comprising two equally spaced gratings followed by a position-sensitive detector. As the beam traverses the moiré setup, $\bar{\text{H}}$ may annihilate on the gratings or nearby structures, producing high-energy pions, or continue towards the position-sensitive detector. For a high-accuracy gravity measurement, precise knowledge of the beam profile and annihilation points is essential. We present results from a feasibility study of vertex reconstruction using modular J-PET detectors spanning the full axial length of the moiré setup. The generated pions, being minimum-ionising particles, follow straight paths. The adapted method is based on the consecutive registration of each pion, defining individual tracks in a pair of modules placed 10 cm apart. The hit positions are used to reconstruct the track direction, which is then projected back to estimate the spatial coordinates of the $\bar{\text{H}}$ annihilation vertex. For this feasibility study, we developed a customised Geant4-based simulation package and an analysis algorithm that implements a track-and-extrapolate algorithm to image the annihilation vertices.

topics: Jagiellonian positron emission tomography (J-PET), antihydrogen, antiproton, annihilation vertex, Antihydrogen Experiment: gravity, Interferometry, Spectroscopy (AE \bar{g} IS)

1. Introduction

The antimatter factory at CERN hosts several complementary experiments (ALPHA-g [1], GBAR [2], AE \bar{g} IS [3]) aiming at the same central question: “How gravity acts on antihydrogen” [4]. Although united by the same goal, these experiments are testing different approaches. The ALPHA-g experiment confines the neutral $\bar{\text{H}}$ and releases them to observe their gravity-driven motion. In the GBAR experiment, the $\bar{\text{H}}^+$ ions are produced following a complex two-step charge-exchange reaction with positronium (Ps), which later converts to $\bar{\text{H}}$ after photo-detachment. The gravity effect will be measured by observing the time-of-flight during free fall.

AE \bar{g} IS follows a completely different approach, based on the production of a pulsed $\bar{\text{H}}$ beam sent through a moiré deflectometer to be registered in a position-sensitive detector with a resolution of a few μm [5]. The gravitational effect can be inferred by measuring the vertical shift in the resulting fringe pattern for two cases, i.e., in the pattern obtained in the presence of the antihydrogen beam and in the pattern obtained using the light source. The $\bar{\text{H}}$ is produced via a charge-exchange process between cold antiprotons and laser-excited Rydberg positronium, as



Positronium atoms are created using nanochanneled silicon e^+ /Ps converters [6], which are subsequently excited to Rydberg states (Ps^*) by laser

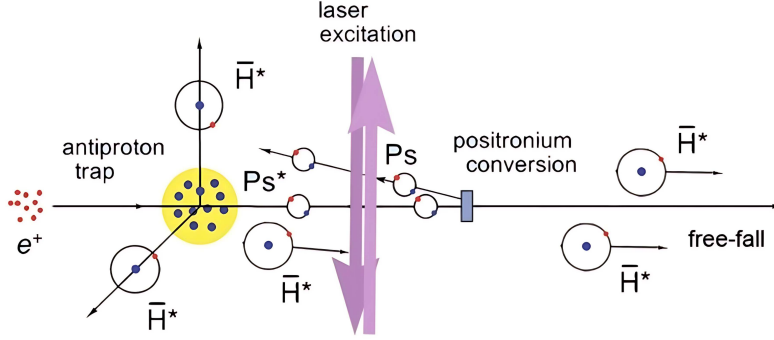


Fig. 1. Schematic of \bar{H}^* production in AEgIS via charge-exchange reaction between trapped antiprotons and laser-excited Rydberg positronium atoms [7].

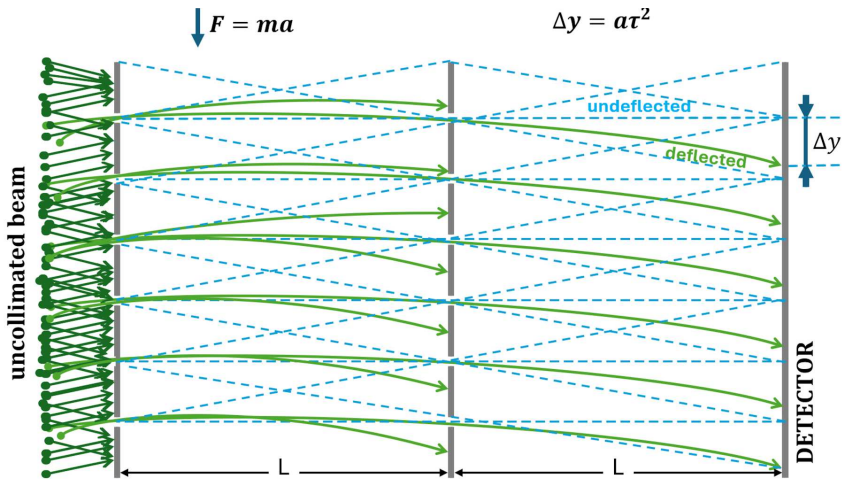


Fig. 2. The difference in trajectories of deflected particles (solid green lines) and undeflected photons (dashed blue lines) from a multiple slit grating.

manipulation, thereby producing an approximately isotropic, pulsed \bar{H} with a well-defined formation time. The scheme of producing the \bar{H} beam is shown in Fig. 1 (see also [7]).

The \bar{H} produced with a velocity determined mainly by the \bar{p} velocity is transported to the moiré deflectometer for gravity measurements [8]. The moiré deflectometer consists of two equally spaced gratings made of silicon wafers with a slit width of $40 \mu\text{m}$ and a period of $100 \mu\text{m}$ [9]. The \bar{H} beam spans a path of $\approx 100 \text{ cm}$ before being detected by a highly sensitive position-sensitive detector (OPHANIM — Optical Photon and Antimatter Imager) at the end of the moiré deflectometer [10], which is a customizable detector system consisting of 3840-Megapixel CMOS sensors, sensitive to both light and particles that annihilate on it [11].

During the passage of \bar{H} through the moiré deflectometer, two gratings impose a modulation recorded by the OPHANIM. The statistically inferred fringe pattern [12] will be compared with that obtained from a reference light source under the same experimental conditions. Any observed shift (Δy) will be the measure of the gravity-induced

effect on \bar{H} . The paths modulated by the gratings for the light source (dashed blue lines) and the \bar{H} beam (solid green lines) are shown in Fig. 2.

For the proper diagnosis of the \bar{H} beam, two additional detection systems are planned to be commissioned. First, SARA (Scintillator Assemblies to Reveal Annihilations) box scintillators will be placed to scan the expected annihilation spots [13] around the gratings and at the OPHANIM detector position. In this configuration, SARA will not only register the annihilations but also provide the time-of-flight information. Second, to reconstruct the vertices of annihilated \bar{H} during its passage through the moiré setup, four Jagiellonian positron emission tomography (J-PET) [14–16] detection units will be placed in a pair-wise configuration, covering almost the entire length of the moiré setup.

In this work, we present the results of a feasibility study on reconstructing annihilation vertices based on Geant4 simulations [17]. Although \bar{H} annihilations yield various secondary particles, we illustrate the method using an exemplary monoenergetic charged pion passing subsequently through two modules of either pair.

2. Modular J-PET

J-PET is a plastic scintillator-based detection technology optimised for fast timing and covering a wide field of view [18]. Modular J-PET refers to the new prototype consisting of 24 detection modules that can be arranged in multiple configurations [14, 19–21]. The original concept was to build a plastic scintillator-based PET scanner, in which all modules can be arranged in a cylindrical configuration. However, thanks to the modular design, each module can also be used as a standalone detection unit, easily portable outside of the J-PET laboratories. Each module consists of 13 BC-404 plastic scintillators ($6 \times 24 \times 500 \text{ mm}^3$). The scintillators are read out by a 1×4 matrix of silicon photomultipliers (SiPMs). The J-PET technology is based on triggerless and reconfigurable data acquisition, allowing multiple particles to be registered simultaneously [22]. The readout at both ends of the 500 mm long strip (the z coordinate) allows one to determine the hit-position and hit-time by calculating the time difference between the light signals arriving at the two ends [23].

Within the framework of the $AE\bar{g}IS$ Collaboration, four dedicated standalone detection modules based on J-PET technology were assembled for integration with the SARA and OPHANIM detectors around the moiré setup to optimise the scanned region of the \bar{H} beam, which was restricted by the inline configuration of the signal readout boards in the original module design. Consequently, the boards were rotated by 90° , as shown in Fig. 3. These modules are easily adaptable to operation

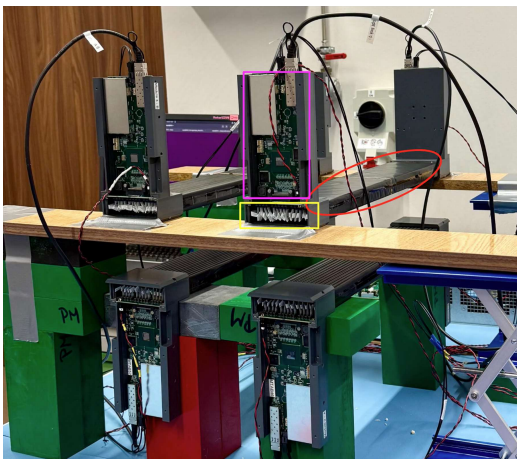


Fig. 3. Laboratory setup of four modules for the calibrations with cosmics. Scintillators are wrapped in black Kapton foils (shown in red oval), and the readout (shown in magenta rectangle) is folded by 90° to reduce the dead zone. The SiPMs are connected to readout via Flat Flexible Cables (shown in yellow rectangle).

Centres of all four modules.

TABLE I

Module	Centre Position (x, y, z)	Side
1	(20.8 cm, 0, 30 cm)	right-front
2	(30.8 cm, 0, 30 cm)	right-back
3	(20.8 cm, 0, -30 cm)	left-front
4	(30.8 cm, 0, -30 cm)	left-back

in the magnetic environment of $AE\bar{g}IS$ and will provide continuous beam monitoring, tracking of secondary particles from \bar{H} annihilations, allowing vertex reconstruction, as well as time-of-flight information.

3. Geant4 simulation for the vertex reconstruction

The simulation was performed using the Geant4 toolkit (v11.2.2) to model the response of the modular J-PET system to secondary particles produced in \bar{H} annihilations within the moiré deflectometer. The present work focused only on tracking the monoenergetic pions. The main objectives were:

- (i) to validate the minimum-ionising behaviour of charged pions in the plastic-scintillator modules;
- (ii) to assess the accuracy of a straight line track-and-extrapolate algorithm for annihilation-vertex localisation.

3.1. Geometry and simulation framework

An STL/CAD model of the moiré deflectometer was imported to mimic the experimental setup, allowing us to perform realistic simulations. For the representation of probable annihilation sites, three planes were defined. These planes include two physical gratings and a third plane that coincides with OPHANIM, which acted as an additional annihilation surface in the simulation. For tracking purposes, four J-PET detection modules were used, each module composed of 13 BC-404 scintillator strips (G4_PLASTICSC_VINYLTOLUENE) stacked with a pitch of 1 mm. The modules were placed in pairs along the beam axis to cover the full axial length of the moiré region. The distance between the two modules was fixed at 10 cm. Pairwise placement of the modules allows for the formation of straight-line segments by recording the interaction of pions passing through two modules. Extrapolation of these line segments allowed for the reconstruction of the annihilation vertices. The modules are placed at four different centres, as listed in Table I.

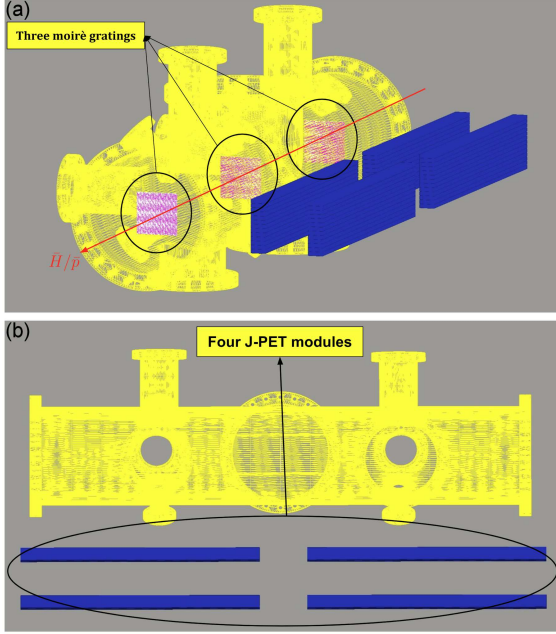


Fig. 4. Schematics showing the placement of J-PET modules along the moiré setup: (a) tilted view of geometry showing the relative grating positions, (b) top view.

Figure 4a shows the imported stereolithography (STL) of the moiré assembly (yellow) together with the detector’s geometry. The placement of the three grating planes (pink) is also shown, indicating the pion-emission positions in the simulation.

Figure 4b presents the top view, highlighting the distances between modules and their offsets from the central axis of the moiré setup.

3.2. Geant4 physics and source definition

In the process of \bar{H} annihilation on a solid target, the positron annihilates with an electron, producing two 511 keV photons, and the antiproton (\bar{p}) annihilates with a nucleus, producing mainly pions (π^\pm, π^0) with an average kinetic energy of 230 MeV [24, 25]. Therefore, in this work, we considered only charged pions with a monoenergetic energy of 230 MeV. In each event, three pions (π^+) are generated simultaneously, one from each grating plane. The geometry of the moiré computer-aided design (CAD) model was centred at the origin (0, 0, 0) of the World volume of Geant4, while the grating planes of dimensions $(7.0 \times 7.0 \times 0.025 \text{ cm}^3)$ were simulated as sources, placed at three different positions (0, 0, -45), (0, 0, 0), and (0, 0, 45). To reduce the computational time, the emission directions were limited to the solid angle subtended by the detector’s geometry. For simulation, we used the physics model FTFP_INCLXX_EMZ, which

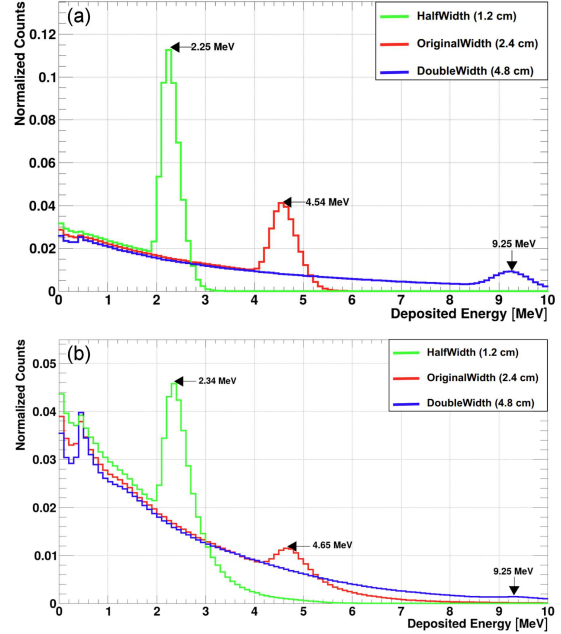


Fig. 5. Mean energy loss of $\sim 1.8 \text{ MeV/cm}$ irrespective of scintillator width, confirming expected MIP behaviour. (a) Energy loss in a single scintillator. (b) Energy loss across four modules.

combines INCL++ [26] for hadronic cascades with G4EmStandardPhysics_option4 for high-precision electromagnetic processes [27].

3.3. Tracking and scoring

A customised primary generator and stepping action class were implemented to record the simulated data. The following key observables were studied:

- **Total energy deposition.**
The energy deposited by particles within the scintillators’ volume was recorded, which served as the primary detector signal.
- **Angular scattering.**
For the positive pions (π^+), the momentum vector was registered upon entering the detector elements to calculate the angular deviation, which is very crucial for performing the vertex reconstruction using the track-and-extrapolate algorithm.
- **Tracking characteristics.**
A detailed trajectory log was written in an external file for further analysis.

4. Results

We first studied the interaction characteristics of π^+ s at 230 MeV energies with BC-404 scintillators as a function of their width. Several key properties

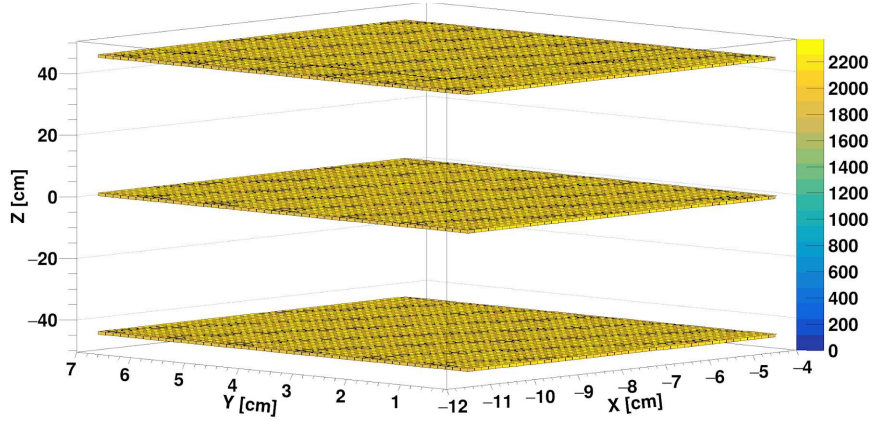


Fig. 6. Spatial distribution of primary particles as generated in Geant4.

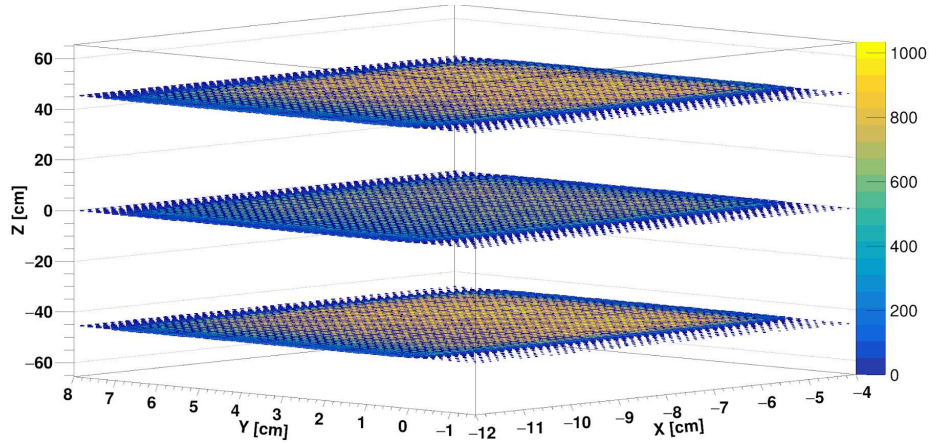


Fig. 7. Distribution of reconstructed vertices after applying the track-and-extrapolate algorithm.

were examined, such as the probability of interaction, the number of interactions per unit length, and the energy deposition per interaction. The simulations were performed for three different widths for a single scintillator, as well as for the cumulative response from all the scintillators of the four modules (see Sect. 4.1). As the next step, we validated the proposed hypothesis to reconstruct the generated vertices by registering the emitted pions subsequently in pair-wise modules (see Sect. 4.2).

4.1. Energy deposition

In Fig. 5, energy deposition as a function of scintillator width is shown. A pion passing through the scintillator medium deposits an amount of energy per unit length of the traversed medium. In the first part of the simulation study, the energy deposition by π^+ as a function of the width of the scintillator was estimated in a single scintillator. In a single scintillator, energy deposition peak for three different widths, i.e., 1.2, 2.4, and 4.8 cm, is

measured at 2.25, 4.54, and 9.25 MeV, respectively, as shown in Fig. 5a. For all four modules, it is measured at 2.34, 4.65, and 9.25 MeV as a cumulative simulated output, as shown in Fig. 5b.

The estimated energy deposition per unit length (peaked values for measured energy deposition divided by the respective scintillator width) is found to be ≈ 1.8 MeV/cm. This result is in good agreement with the expected energy loss for minimum ionising particles (MIPs) in organic scintillators [28].

4.2. Algorithm for the vertex reconstruction

To validate the hypothesis of vertex reconstruction based on the simultaneous registration of pions in consecutive modules (of an individual pair), a C++/ROOT-based algorithm (track-and-extrapolate algorithm) was developed. In the simulated output, several required pieces of information were extracted event-wise for registered particles, such as `event_ID`, `track_ID`, hit-coordinates,

scintillator_IDs, energy deposition, and momentum directions. For the analysis, events with only two hits were considered qualified under the following assumptions:

- The registered hits come from a given pair of modules, based on pre-defined scintillator_IDs.
- Both hits caused by the same particle can be confirmed by using their unique track_IDs.
- A single interaction takes place per module.

After selecting the events of interest, our algorithm determines the pion trajectory based on the line segment created using the 3D coordinates of both hits. Later, this line was extrapolated towards the moiré setup, and the algorithm tests for geometric intersection with any of the three sources (grating) of pion generation. If the interaction is successful, the intersection point is recorded as the reconstructed vertex, while these tracks become ineligible for further analysis when no interactions occur. The vertices of the generated particles were also stored to be used as the ‘ground truth’, and the performance of vertex reconstruction was calculated. The generated distribution of the vertices is presented in Fig. 6. It shows the spatial distribution of primary particles generated in Geant4 with sources centred at $z = -45$ cm, $z = 0$ cm, and $z = 45$ cm.

Figure 7 shows the distribution of vertices after applying the track-and-extrapolate reconstruction algorithm to the simulated detector data. The algorithm successfully resolves the three distinct source planes, demonstrating the viability of the proposed algorithm. By comparing the generated and reconstructed vertices for pions originating from different grating positions, one can also estimate the efficiency of the developed algorithm.

5. Conclusions

We present a feasibility study for reconstructing the annihilation vertices of the \bar{H} beam inside the AE \bar{g} IS moiré deflectometer using modular J-PET detectors. The preliminary results were obtained with a Geant4 application that models charged pions originating from three sources (gratings). This study confirms that charged pions exhibit minimum-ionising behaviour in BC-404 plastic scintillators, by losing energy at about 1.8 MeV/cm, which matches the predicted behaviour for plastic scintillators. Furthermore, a method based on a track-and-extrapolate algorithm was demonstrated to determine the spatial coordinates of the annihilation points from coincident hits in consecutive J-PET modules. These findings demonstrate that the modular J-PET system has the potential to perform precise tracking and vertex localisation

of secondary particles resulting from antihydrogen annihilation, complementing the other detection systems, i.e., SARA and OPHANIM.

Acknowledgments

We acknowledge support from the National Science Centre of Poland through grants SONATA Bis no. 2023/50/E/ST2/00574, the Ministry of Science and Higher Education through grant no. IAL/SP/596235/2023, the SciMat and qLife Priority Research Areas budget under the program Excellence Initiative — Research University at Jagiellonian University, the Research Support Module as part of the Excellence Initiative — Research University program at Jagiellonian University in Kraków.

References

- [1] C. Amole, M.D. Ashkezari, M. Baquero-Ruiz et al., *Nat. Commun.* **4**, 1785 (2013).
- [2] P. Pérez, D. Banerjee, F. Biraben et al., *Hyperfine Interact.* **233**, 21 (2015).
- [3] D. Krasnický, S. Aghion, C. Amsler et al., *AIP Conf. Proc.* **1521**, 144 (2013).
- [4] S.G. Karshenboim, *J. Phys. B At. Mol. Opt. Phys.* **49**, 144001 (2016).
- [5] M. Doser, C. Amsler, A. Belov et al., *Class. Quantum Grav.* **29**, 184009 (2012).
- [6] S. Mariazzi, R. Caravita, M. Doser, G. Nebbia, R.S. Brusa, *Eur. Phys. J. D* **74**, 79 (2020).
- [7] R. Caravita (on behalf of the AE \bar{g} IS Collaboration), [arXiv:2208.07050](https://arxiv.org/abs/2208.07050) (2022).
- [8] C. Amsler, M. Antonello, A. Belov et al., *Commun. Phys.* **4**, 19 (2021).
- [9] K. Jefimovs, L. Romano, J. Vila-Comamala, M. Kagias, Z. Wang, L. Wang, C. Dais, H. Solak, M. Stampanoni, in: *Advances in Patterning Materials and Processes XXXIV*, Vol. 10146, SPIE, 2017, p. 101460L.
- [10] R.C. Ferguson, S. Alfaro Campos, M. Auzins et al., *J. Phys. Conf. Ser.* **3029**, 012005 (2025).
- [11] M. Berghold, D. Orsucci, F. Guatieri et al., *Sci. Adv.* **11**, eads1176 (2025).
- [12] S. Aghion, O. Ahlén, C. Amsler et al., *Nat. Commun.* **5**, 4538 (2014).
- [13] P. Conte, G. Consolati, M. Prata et al., [arXiv:2506.09274](https://arxiv.org/abs/2506.09274) (2025).
- [14] P. Moskal, J. Baran, S. Bass et al., *Sci. Adv.* **10**, eadp2840 (2024).

- [15] P. Moskal, E. Czerwiński, Juhi Raj et al., *Nat. Commun.* **15**, 78 (2024).
- [16] S. Sharma, L. Povolo, S. Mariazzi et al., *Nucl. Instrum. Methods Phys. Res. A* **1062**, 169192 (2024).
- [17] S. Agostinelli, J. Allison, K. Amako et al., *Nucl. Instrum. Methods Phys. Res. A* **506**, 250 (2003).
- [18] P. Moskal, O. Rundel, D. Alfs et al., *Phys. Med. Biol.* **61**, 2025 (2016).
- [19] M. Das, R. Bayerlein, S. Sharma et al., *Bio-Algorithms Med-Syst.* **20**, 101 (2024).
- [20] P. Moskal, E. Stępień, A. Khreptak, *Bio-Algorithms Med-Syst.* **20**, 55 (2024).
- [21] F. Tayefi Ardebili, P. Moskal, *Bio-Algorithms Med-Syst.* **20**, 1 (2024).
- [22] G. Korcyl, D. Alfs, T. Bednarski et al., *Acta Phys. Pol. B* **47**, 491 (2016).
- [23] S. Sharma, K. Kacprzak, K. Dulski et al., *J. Phys. Conf. Ser.* **2374**, 012040 (2022).
- [24] E. Klempt, C. Batty, J. Richard, *Phys. Rep.* **413**, 197 (2005).
- [25] C. Amsler, *Rev. Mod. Phys.* **70**, 1293 (1998).
- [26] D. Mancusi, A. Boudard, J. Cugnon, J.-C. David, P. Kaitaniemi, S. Leray, *Phys. Rev. C* **90**, 054602 (2014).
- [27] C. Amsler, H. Breuker, M. Bumbar et al., *Eur. Phys. J. A* **60**, 225 (2024).
- [28] J. Apilluelo L. Asquith, E.F. Bannister et al., [arXiv:2507.13864](https://arxiv.org/abs/2507.13864) (2025).